Deriving the hygroscopicity of ambient particles using low-cost optical particle counters

Wei-Chieh Huang[1], Hui-Ming Hung[1*], Ching-Wei Chu[1], Wei-Chun Hwang[1], and Shih-Chun Candice Lung[2]

[1]Department of Atmospheric Sciences, National Taiwan University, Taipei, 106319, Taiwan
[2] Research Center for Environmental Changes, Academia Sinica, Taipei, 115201, Taiwan

Correspondence to: Hui-Ming Hung (hmhung@ntu.edu.tw)

Abstract. This study investigates the chemical composition and physical properties of aerosols, which play a crucial role in influencing human health, cloud physics, and local climate. Our focus centers on the hygroscopicity of ambient aerosols, a key property reflecting the ability to take up moisture from the atmosphere, and serve as cloud condensation nuclei. Employing home-built Air Quality Box (AQB) systems equipped with low-cost sensors, we assess the ambient variability of particulate matter (PM) concentrations to determine PM hygroscopicity. The AQB systems effectively captured meteorological parameters and most pollutant concentrations, showing high correlations with data from the Taiwan Environmental Protection Administration (TW-EPA). With the application of κ-Köhler equation and certain assumptions, AQB-monitored PM concentrations are converted to dry particle mass concentration, providing optical particles counter sensitivity correction and resulting in improved correlation with TW-EPA data. The derived single hygroscopicity parameters (κ) range from 0.15 to 0.29 for integrated fine particles ($PM_{2.5}$) and 0.05 to 0.13 for coarse particles ($PM_{2.5-10}$), consistent with results of ionic chromatography analysis from a previous winter campaign nearby. Moreover, the analysis of PM_{10} division into $PM_{2.5}$ and $PM_{2.5-10}$, considering composition heterogeneity, provided improved dry PM_{10} concentration as the sensitivity coefficients for $PM_{2.5-10}$ were notably higher than for $PM_{2.5}$. Our methodology provides a comprehensive approach to assess ambient aerosol hygroscopicity, with significant implications for atmospheric modeling, particularly in evaluating aerosol efficiency as cloud condensation nuclei and in radiative transfer calculations. Overall, the AQB systems proved to be effective in monitoring air quality and deriving key aerosol properties, contributing valuable insights into atmospheric science.

List of principle symbols and abbreviations

AQB	Air Quality Box
α	sensitivity coefficient
BAM	Beta Attenuation Mass Monitor
CCN	cloud condensation nuclei
D_{amb}	diameters of the ambient particulate matter
D_d	diameters of the dry particulate matter
DRH	deliquescence relative humidity
E-AIM	the Extended Aerosol Inorganics Model
ε_i	volume fraction of i species
HGF	hygroscopic growth factor
IC	ion chromatography
κ	hygroscopicity (single hygroscopicity parameter)
κ_i	hygroscopicity of i species
ρ_d	density of dry aerosol particles
ρ_w	density of liquid water
M_{BAM}	particulate matter mass concentrations measured by BAM
$M_{d,derived}$	derived dry mass concentration
M_w	molecular weight of water
M_{OPC}	particulate matter mass concentrations measured by optical particle counter
MAPE	mean absolute percentage error
NMHC	non-methane hydrocarbons
OPC	optical particle counter
P	pressure
PM	particulate matter
$PM_{2.5}$	integrated fine particles with a diameter $\leq$ 2.5 µm
$PM_{2.5-10}$	coarse particles with a diameter in a range of 2.5 to 10 µm
R	gas constant (8.314 J $mole^{-1}$ K^{-1})
RH	relative humidity
RI	refractive index
RMSE	root mean squared error
S	water saturation ratio
$\sigma_{s/a}$	surface tension of the particle

T	temperature
TW-EPA	Taiwan Environmental Protection Administration
v_i	volume of i species
v_{total}	total volume of particles

1 Introduction

In an era of increased industrialization, individuals face growing exposure to poor air quality, elevating the risks of cardiovascular and respiratory diseases (Chen et al., 2017; Brook et al., 2010; Heus et al., 2010). Within the realm of air pollutants, atmospheric aerosols emerge as critical components, playing a vital role in Earth's climate system. They influence radiative balance, cloud formation, and precipitation patterns, while significantly impacting human health, visibility, and ecosystems (Pöschl et al., 2010; Wu et al., 2010; Brook et al., 2010; Hamanaka and Mutlu, 2018). Their ability to scatter and absorb solar radiation, coupled with their role as cloud condensation nuclei (CCNs), emphasizes their significance in shaping both climate dynamics and air quality (Andreae and Rosenfeld, 2008; Rosenfeld et al., 2014; Lohmann and Feichter, 2005). However, understanding the complex interplay between aerosols and these processes requires the physical and chemical properties of aerosols, including hygroscopicity. The hygroscopic growth of aerosol particles, indicating their ability to take up moisture from the ambient air, alters their size distribution, mass, optical properties, and CCN activity, thereby impacting climate dynamics and air quality (Petters and Kreidenweis, 2007). The traditional methods such as hygroscopicity tandem differential mobility analyzers and cloud condensation nuclei counters (Chan and Chan, 2005; Hung et al., 2016; Bian et al., 2014) have provided valuable insights into the hygroscopic properties of various aerosol types. However, their complexity and cost often limit their applicability for extensive, long-term measurements.

Over the past decade, the rise in popularity of low-cost optical particle counter (OPC) can be attributed to their simplicity, portability, and affordability (Sá et al., 2022; Crilley et al., 2018; Samad et al., 2021). OPCs provide real-time data on particle size distributions and mass concentrations with high temporal resolution for monitoring ambient particles. However, challenges arise in ensuring the accuracy of OPCs, necessitating additional constraints or calibrations for optimal performance. The measurement principle of OPCs relies on the dependence of Mie scattering on particle size, yet this dependence is non-monotonic across all sizes. Additionally, particle composition influences light scattering, leading to varying scattering efficiencies (Kaliszewski et al., 2020; Formenti et al., 2021). Variations in particle density directly affect the mass concentration derived from the monitored number size concentration (Hagan and Kroll, 2020; Dacunto et al., 2015). A particularly challenging issue involves the removal of liquid water from ambient particles. Several studies have attempted to derive the dry mass concentration of ambient particles using OPC, employing calibration methods linked to the hygroscopic growth factor (HGF) under controlled relative humidity (RH) conditions. Notably, Crilley et al. (2018) improved OPC mass concentration correction by applying the derived hygroscopicity (κ) values of 0.38-0.41 and 0.48-0.51 for $PM_{2.5}$ and PM_{10}, respectively, achieving a 33% improvement. Similarly, Antonio et al. (2018) and Jagatha et al. (2021) elevated calibration from a moderate to a high correlation by assuming a constant κ of 0.40. Furthermore, the chemical composition and physical properties of aerosols exhibit high temporal-spatial variation, making the analysis and correction of observational data from a physical perspective crucial. The widespread adoption of low-cost sensors, attributed to their affordability, enables more extensive use as users find them more accessible (Castell et al., 2017). This increased utilization enhances spatial resolution in

environmental monitoring, deepening our understanding of pollution evolution. However, it is essential to emphasize that regular maintenance and calibration are necessary for accurate results (Concas et al., 2021; Sá et al., 2022).

In this study, we evaluate the performance of our home-built monitoring system, Air Quality Box (AQB), through a comprehensive analysis and calibration by co-locating them with the Taiwan Environmental Protection Administration (TW-EPA) station. Our primary focus is on OPC, for which we employed a physical model to elucidate the hygroscopic characteristics of ambient particles during the determination of dry particle mass concentrations for integrated fine particles ($PM_{2.5}$, $D_p \leq 2.5$ μm) and coarse particles ($PM_{2.5-10}$, 2.5 μm $< D_p \leq 10$ μm), respectively. Additionally, we discuss various factors contributing to errors in hygroscopicity estimates, aiming to gain valuable insights into using low-cost sensors for extensive and prolonged monitoring applications.

2 Methodology

2.1 Air Quality Box (AQB) system

Two home-built AQB systems (AQB #1 and AQB #2) consist of multiple sensors that monitor meteorological parameters such as temperature (T), relative humidity (RH), and pressure (P), as well as gaseous species, and particulate matter (PM) with a temporal resolution of seconds as shown in Fig. 1 with sensor information summarized in Table S1. The gas sensors include five Alphasense amperometric B4 series sensors that measure CO, NO, NO_2, Ox (O_3+NO_2), and SO_2, a photo-ionization detector (PID-AH2, Alphasense) monitoring volatile organic compounds, and a non-dispersive infrared CO_2 sensor from Amphenol Advanced Sensors (T6713-5K). The PID sensor, equipped with a Krypton lamp providing a photon energy of about 10.6 eV, cannot detect methane, which has a higher ionization potential of ~13.7 eV (Glockler, 1926). Therefore, the data of non-methane hydrocarbons (NMHC) from TW-EPA is more comparable to PID data in our analysis. The PM sensor (OPC-N2, Alphasense), an optical particle counter, monitors the number size distribution between 0.38 and 17 μm, divided into 16 bins based on Mie scattering, with a sampling flow rate of ~4 mL s^{-1} and a refractive index of 1.5+0 i. In addition, the mass concentration of PM_1, $PM_{2.5}$, and PM_{10} could be calculated from the number size distribution, assuming a particle density of 1.65 g cm^{-3}. These sensors were controlled by a small single-board computer, Raspberry Pi Zero W, at a time resolution of 3 s with data stored in a microSD card and uploaded to cloud storage via 4G LTE. The entire system is housed in a remodeled enclosure with a dimension of 25 cm × 16 cm × 8 cm (L × D × H) and has well-ventilated openings for sampling and exhaust. The sampling flow rate is primarily controlled by an installed fan at ~ 5.6 L min^{-1}, corresponding to a residence time of approximately 34 s in the box. This configuration allows the system to effectively monitor ambient air quality independently without the need of additional inlets.

2.2 Calibration campaign and reference data

The calibration of AQB sensors was carried out by co-locating them with TW-EPA Nanzi station (Fig. S1) in Kaohsiung, Taiwan (22°44'12" N, 120°19'42" E) from 4 to 19 February 2021. Nanzi station is situated on the roof of a 15 m high building in a well-ventilated environment. The primary gaseous components, dry $PM_{2.5}$ and PM_{10} concentrations, and basic meteorological parameters are continuously monitored using standard instruments, as summarized in Table S1. For electrochemical sensors in AQB, the performance can be influenced by environmental parameters such as temperature, relative humidity, and other chemical species that have high cross-sensitivity (Concas et al., 2021; Karagulian et al., 2019; Mead et al., 2013). Therefore, in this study, a linear regression with a multivariate function of voltage and the environmental temperature was applied to retrieve concentrations for gas species. For PM, the reported values by Beta Attenuation Mass Monitor (BAM) in the TW-EPA station reflect the dry-state PM concentration by controlling the measurement at RH less than 50% (i.e., a heating device applied to reduce the sampling flow to 35% water saturation when the ambient RH is > 50%). On the contrary, the optical particle counter (OPC) in AQB directly monitors ambient PM concentration. The difference between BAM and OPC data reflects the amount of liquid water content in ambient conditions. A simple linear regression between them might not completely reveal the influence of hygroscopicity. Therefore, the κ-Köhler equation (Petters and Kreidenweis, 2007) was applied to derive the κ as discussed in the following section.

2.3 Sensitivity coefficients of OPCs and particle hygroscopicity

To bridge the PM concentration gap between BAM and OPC, the sensitivity correction of OPC and the conversion of ambient particles to dry particles are required. The sensitivity coefficient (α) was evaluated as the mass concentration ratio of BAM and OPC data at low RH (≤ 50%) having limited water content, as follows:

$$\alpha = \frac{M_{BAM}}{M_{OPC}} \quad (1)$$

where M_{BAM} and M_{OPC} are PM mass concentrations (μg m^{-3}) measured by BAM and OPC, respectively. RH ≤ 50% was applied as the threshold criteria for data selection to determine α, as the mass concentration of ambient particles might have significant water uptake at higher RH. The statistical distribution of M_{BAM} to M_{OPC} ratios at RH ≤ 50% was analyzed to assign α as the mean value ± 0.5σ (σ: standard deviation) to prevent high-concentration data points from dominating the statistical result.

The particle size growth with the water saturation ratio (S) for a given κ can be evaluated using κ-Köhler equation as follows (Petters and Kreidenweis, 2007):

$$S = \frac{D_{amb}^3 - D_d^3}{D_{amb}^3 - D_d^3(1-\kappa)} exp\left(\frac{4\sigma_{s/a} M_w}{R\,T\,\rho_w D_{amb}}\right) \quad (2)$$

where D_{amb} and D_d are the diameters (m) of the ambient and dry particulate matter, respectively, $\sigma_{s/a}$ is the surface tension of

the particle (J m^{-2}), M_w is the molecular weight of water (g $mole^{-1}$), R is the gas constant (J $mole^{-1}$ K^{-1}), T is the temperature, and ρ_w is the density of liquid water (1.0 g cm^{-3}). The first term is the solute effect, while the second is the Kelvin effect. As the mass is dominated by the larger particles, the Kelvin effect in Eq. (2) is assumed to be negligible for simplification. The derived dry mass concentration ($M_{d,derived}$) from the measured ambient particles from OPC data can be expressed as follows (Pope et al., 2010; Crilley et al., 2018):

$$M_{d,derived} = (\alpha \times M_{OPC}) \times \left[\left(\frac{S\,\kappa}{1-S}\right) \times \frac{\rho_w}{\rho_d} + 1\right]^{-1} \quad (3)$$

where ρ_d is the density of dry aerosol particles and is assumed to be 1.20 g cm^{-3} in this study. With the determined α values (Eq. (1)), κ can be derived from the data points of aqueous particles at RH above 70%, the deliquescence RH (DRH) verified using ion chromatography (IC) analyzed composition with the Extended Aerosol Inorganics Model (E-AIM) model. The mean absolute percentage error (MAPE) parameter between $M_{d,derived}$ and M_{BAM} was used to assess the appropriate κ value as follows:

$$MAPE = \frac{\sum_{i=1}^{n} \frac{\left|M_{d,derived,i} - M_{BAM,i}\right|}{M_{BAM,i}}}{n} \times 100\% \quad (4)$$

where n is the total number of data points. With the restricted range of α, κ can be derived under the minimum MAPE. The detailed process description for κ derivation is provided in the supplementary material. Due to the heterogeneity between particles, PM_{10} was divided into integrated fine particles ($D_p \leq 2.5$ μm) and coarse particles (2.5 μm < $D_p \leq 10$ μm) to evaluate the individual sensitivity coefficient and hygroscopicity.

2.4 Composition analysis

Hygroscopicity can also be determined using the volume fraction of the major components. Based on an earlier field campaign, the ion chromatography (IC) method was applied to quantify water-soluble components for samples (both $PM_{2.5}$ and PM_{10}) collected at Fooyin University (22°36'09.8" N, 120°23'23.1" E) in Kaohsiung from 15 to 28 January 2013. Ambient aerosol samples were collected using a pair of dichotomous aerosol samplers (Model: RP-2025, R&P Co., Inc., Albany, New York) to collect integrated fine and coarse particles on Teflon filters with sampling flow rates of 15.0 and 16.7 L min^{-1}, respectively. The samples were categorized into daytime and nighttime. Daytime samples were collected from 08:00 to 20:00 LT, and nighttime samples were collected from 20:00 to 08:00 LT the next day. The samplers were equipped with Teflon filters deployed for the measurement of water-soluble ions (Na^+, Mg^{2+}, K^+, Ca^{2+}, NH_4^+, Cl^-, SO_4^{2-}, and NO_3^-) via ion chromatography (Model: ICS 1000, Dionex). More information on the chemical analysis method can be found in Salvador and Chou (2014). To derive the hygroscopicity from samplings, the ions from IC analysis were converted to chemical components via the following sequence: ammonium sulfate, ammonium bisulfate, ammonium nitrate (when there is residual ammonium), sodium nitrate, and sodium chloride. With the assumption of the hygroscopicity of insoluble components as zero and negligible

residual ions contribution (less than 5% of total mass), the overall hygroscopicity can be derived by the volume fraction (ε_i) weighted hygroscopicity from individual soluble component (*i* species) as follows:

$$\kappa = \sum_i \varepsilon_i \kappa_i = \sum_i \frac{v_i}{v_{total}} \kappa_i \quad (5)$$

where κ_i is the hygroscopicity of *i* species, v_{total} is the volume of particles, and v_i is the volume of *i* species. The conversion of particle mass to volume is based on a density of 1.20 g cm^{-3}. The applied hygroscopicity, molecular weight, and density for the related chemical species are summarized in Table S2. With the assumption that these ions dissolve completely in the aqueous phase, which represents the maximum estimation, the hygroscopic contributed by the residual ions were found to be approximately up to 1.8% and 6.4% of the overall κ value for integrated fine particles ($PM_{2.5}$) and coarse particles ($PM_{2.5-10}$), respectively. Given their limited impact on the hygroscopic behavior of the particles, the contribution of the residual ions was not taken into account in the calculation. Additionally, another $PM_{2.5}$ IC data for samples collected at the National Kaohsiung University of Science and Technology (22°46'22.4" N, 120°24'03.4" E) in Kaohsiung for the period of 8 – 18 December 2021smaples was also applied for further comparison (no PM_{10} collection for that campaign). We opted for the 2013 dataset for more discussion due to its comprehensive analysis encompassing both $PM_{2.5}$ and $PM_{2.5-10}$. Furthermore, the composition data obtained from IC analysis was applied to E-AIM Model III (for systems containing H^+, NH_4^+, Na^+, SO_4^{2-}, NO_3^-, Cl^-, and H_2O) to evaluate the characteristics of volume variation as a function of RH in the range of 30 to 90% (Clegg et al., 1998). The partitioning of selected trace gases (HNO_3, HCl, NH_3, and H_2SO_4) into the vapor phase was disabled to keep a consistent quantity of applied chemical species in the particle phase. The growth factor, V_{amb}/V_d, above DRH, was applied to retrieve κ value using Eq. (2) but without the Kelvin effect term (Luo et al., 2020). Both the individual sample concentrations and the overall averaged composition conditions were analyzed to evaluate the hygroscopic behavior of the particles.

3 Results and Discussion

3.1 Performance of AQB systems

Figure 2 shows the time series of the meteorological parameters and pollutant concentrations between calibrated AQB and TW-EPA data from 14 to 17 February 2021. T, RH, CO, and Ox showed a good correlation with r > 0.9, while NO, NO_2, $PM_{2.5}$, and PM_{10} had a moderate correlation (r ≥ 0.48). The high correlation (r=0.976) for CO (with a lifetime of ~ 2 months) indicates a similar air parcel sampled by both AQB and the instrumentation in TW-EPA. The PID sensor had consistent peaks with high NMHC concentrations and could not reveal temporal variation at low concentrations, resulting in a low correlation. Overall, the AQB system performs well in capturing the ambient variability of pollutants stated above. The low correlation of SO_2 was due to the cross-sensitivity of this SO_2 sensor, which was highly sensitive to O_3 and NO_2 (about -120% reported in the Technical Specification of Alphasense). O_3 and NO_2 generally have higher concentrations than SO_2 and cause a significant contribution to the response of the SO_2 sensor. However, if high SO_2 concentration events occur, the SO_2 sensor might reflect the variation of SO_2 concentration. The PM concentration shown in Fig. 2 was calibrated using a simple linear regression,

which roughly reflects the trend of mass concentration but shows more significant deviations at higher RH due to more water uptake in particles, as discussed in Sect. 3.2. Most gas species showed a high correlation ($r \geq 0.95$) between different AQB systems except for NMHC ($r = 0.675$) as summarized in Table S3. Further results and discussions focus on the PM analysis using AQB #1, which has a more consistent sampling rate during the observation period, unless stated otherwise.

3.2 Comparison between OPC and BAM data

3.2.1 Sensitivity coefficient of OPC

Figures 3(a) and 3(c) show the scatter distribution of the mass concentrations between OPC (with no calibration) and BAM data for $PM_{2.5}$ and PM_{10}, respectively. Overall, the PM mass concentrations measured by OPC have a similar trend to those measured by BAM, but exhibit some variability. The results reveal an apparent influence of ambient RH, indicating the contribution of water content. The red-shaded area represents a regression line with a slope corresponding to the inverse of the α derived from data points at ambient RH $\leq$ 50% (17 out of 356 points, 5%). The notable deviation of the red shaded area from the 1:1 line towards the right side indicates the requirement of $\alpha > 1$ corrections, contributed by the different measurement principles and calibration techniques, which may result from the assumed particle density and refractive index (RI) (dust, density: 1.65 g cm^{-3}, RI: 1.5 + 0i). The estimated α, as summarized in Table 1, are higher for PM_{10} than for $PM_{2.5}$, i.e., 2.02 ± 0.34 vs 1.26 ± 0.16, which are reasonably conclusive as tested with more data points selected at higher RH thresholds (Fig. S2). The α difference between $PM_{2.5}$ and PM_{10} might be attributed to the complex composition of ambient particles, which differs from the samples used for instrument calibration, as well as possible sensitivity variations in OPC over time. With sensitivity calibration, the performance at ambient RH $\leq$ 50% exhibits a strong correlation with MAPE at 12.8%, 18.5%, and root mean squared error (RMSE) at 3.7 μg m^{-3}, 10.3 μg m^{-3} for $PM_{2.5}$ and PM_{10}, respectively, as summarized in Table 2 excluding the two significant outliers (shown as hollow circles in Fig. 3). The results confirm the effectiveness of OPCs in capturing PM concentrations after proper calibration, consistent with other real-time outdoor field studies, reporting R^2 ranging from 0.34 to 0.97, RMSE ranging from 0.52 to 12.3 μg m^{-3}, and MAPE about 22% (Gillooly et al., 2019; Demanega et al., 2021; Sá et al., 2022; Crilley et al., 2018). Additionally, the OPC sampling flow rate has an impact on measurement performance. AQB #1 maintained a steady rate at 3.6 ± 0.2 LPM, whereas AQB #2 exhibits two distinct periods with sampling flow rates of 3.6-4.2 LPM for the first period and 3.2-3.6 LPM for the second period. The distinctive sampling flow rates result in a non-linear change in α, suggesting the need to separate the data into two parts to estimate the individual α (Fig. S3).

3.2.2 Hygroscopicity derivation

With the derived α, the hygroscopicities were retrieved using Eq. (3), resulting in κ ranging from 0.18 to 0.29 for $PM_{2.5}$ and 0.20 to 0.39 for PM_{10} during the studied period, as summarized in Table 1. Figures 3(d) and 3(f) show the scatter distribution of the derived dry concentration vs. BAM concentration for $PM_{2.5}$ and PM_{10}, respectively. The results from the two OPCs exhibit slight differences but are consistent overall. Considering both the sensitivity coefficient and hygroscopicity, the

performance of OPC in deriving dry PM concentration is significantly improved with lower MAPE, RMSE, and higher R^2 than the results obtained using only the sensitivity coefficient, as summarized in Table 2. With a similar methodology, Crilley et al. (2018) applied κ-Köhler equation to compare measured data between OPC-N2 and tapered element oscillating microbalance (TEOM) and derived the κ ranging from 0.38 to 0.41 and 0.48 to 0.51 for $PM_{2.5}$ and PM_{10}, respectively, which is within the range for Europe (i.e., 0.36±0.16) (Pringle et al., 2010).

Due to the heterogeneity of composition among different sizes, PM_{10} can be divided into $PM_{2.5}$ and $PM_{2.5\text{-}10}$ for further analysis. The estimated α value for $PM_{2.5\text{-}10}$, as summarized in Table 1, is approximately one order of magnitude higher than that for $PM_{2.5}$. The lower κ for $PM_{2.5\text{-}10}$ might suggest a significant contribution from dust or other less hygroscopic species, consistent with the IC analyses in Table 3 and discussed further in Sect. 3.3. With the retrieved α and κ for $PM_{2.5}$ and $PM_{2.5\text{-}10}$, Fig. 3(e) shows the scatter distribution between the derived dry $PM_{2.5\text{-}10}$ from OPC and BAM data, exhibiting a MAPE of 31.8%, more significant than the 24.8% for $PM_{2.5}$. The higher MAPE might result from the low particle number concentration in the coarse mode, with only about 0.01 to 0.1 particles per bin cm^{-3} in the size range of 3.0 to 10.0 μm. The results are consistent with the findings of Kaliszewski et al. (2020), which showed that the correlation between OPC-N3 (a newer version of OPC-N2) and AeroTrak 8220 (TSI INC., Shoreview, MN, USA) measurement data decreases with particle size, from 0.3-0.5 μm (r=0.99) to 5-10 μm (r=0.74). The dry PM_{10} derived from OPC through the divided $PM_{2.5}$ and $PM_{2.5\text{-}10}$ analysis demonstrates better consistency with the reported BAM data than the direct calibration method. This is evidenced by a lower MAPE in Fig. 3(g) (18.2%) compared to Fig. 3(f) (29.2%) and a significant improvement than the simple linear regression method, which has a higher MAPE at 62.5% (Table 2). Moreover, the derived κ for PM_{10} with the size-dependent sensitivity coefficient correction ranges from 0.13 to 0.23 (Table 1). This value falls between those for $PM_{2.5}$ and $PM_{2.5\text{-}10}$ and is more reasonable compared to κ derived with a fixed sensitivity coefficient (κ = 0.20-0.39, higher than those for $PM_{2.5}$ and $PM_{2.5\text{-}10}$). The results substantiate the importance of considering composition heterogeneity among particle sizes for accurate dry PM derivation.

3.3 Hygroscopicity derivation using IC data

3.3.1 Composition analysis

The major soluble composition and concentrations obtained from the IC analysis are summarized in Table 3. The mean concentrations of $PM_{2.5}$ and $PM_{2.5\text{-}10}$ are 67 ± 19 and 36 ± 7 μg m^{-3}, respectively. The determined soluble composition of $PM_{2.5}$ constitutes approximately 53% of the mass fraction and is predominantly composed of NH_4^+, SO_4^{2-}, and NO_3^-, which are formed through chemical reactions involving industrial and agricultural emissions. In contrast, ~30% of $PM_{2.5\text{-}10}$ is soluble components, including NO_3^-, SO_4^{2-}, Na^+, Cl^-, NH_4^+, and some alkaline earth metal ions (Ca^{2+} and Mg^{2+}), with a more significant proportion being insoluble components (~70%), likely attributed to dust, metallic elements, and unanalyzed organic components. The higher portion of sea salt (Na^+ and Cl^-) in $PM_{2.5\text{-}10}$ than in $PM_{2.5}$ is likely transported by the sea breeze during the daytime, while the increased fractions of Ca^{2+} and Mg^{2+} might correspond to sand or dust particles (Li et al., 2022).

The temporal variation of derived κ, based on the IC soluble composition analysis, ranges from 0.14 to 0.26 for $PM_{2.5}$ and 0.06 to 0.21 for $PM_{2.5-10}$, as shown in Fig. S4(a) and summarized in Table 1. A similar analysis for the winter of 2021 showed a similar κ range for $PM_{2.5}$, as illustrated in Fig. S5. This consistency across distinct study periods indicates typical winter hygroscopic characteristics for ambient $PM_{2.5}$ in Kaohsiung City, applicable for further discussion with the OPC data. For $PM_{2.5-10}$, the more significant variability in κ compared to $PM_{2.5}$ can be attributed to substantial fluctuations of soluble composition in coarse particles, primarily driven by significant quantities of thenardite (Na_2SO_4) and halite (NaCl) (Tang et al., 2019). Due to the dominance of the northeast monsoon wind during the filter sampling period, the influence of the sea-land breeze was relatively weak to cause apparent diurnal variation in κ.

The κ values derived from IC analysis reflect the temporal variation, while those from OPC analysis indicate the overall physical properties of ambient aerosols for the studied period. Factors such as spatial and temporal variations in aerosols, different campaign years and locations (~20 km apart, as shown in Fig. S1), and technique uncertainties, such as ammonia and nitrate sampling evaporation during filter sampling (Hering and Cass, 1999; Chen et al., 2021), as well as OPC detection uncertainties and assumption required for calculation, can influence comparisons. However, the results (i.e., ~0.22 (OPC) vs. 0.14-0.27 (IC) for $PM_{2.5}$ and ~0.09 (OPC) vs. 0.06-0.21 (IC) for $PM_{2.5-10}$) summarized in Table 1 and Fig. 4(a) suggest that the derived κ values from OPC data likely reflect the mean hygroscopicity for the integrated fine and coarse particles during winter in Kaohsiung City.

3.3.2 E-AIM analysis

With the measured composition, the hygroscopicity can be derived from the growth pattern. The particle growth might follow the κ-Köhler equation (Eq. (2)) when all soluble species are fully dissolved, typically occurring above the DRH. Using the averaged soluble composition determined from the IC analysis, HGF as a function of RH calculated using E-AIM is shown in Fig. 5. For $PM_{2.5}$, partial deliquescence initiates at 60% of RH with some residual solid components such as ($(NH_4)_2SO_4$ and $2NH_4NO_3.(NH_4)_2SO_4$). Complete dissolution occurs at RH ~72%. In the case of $PM_{2.5-10}$, water uptake begins at 42% RH, leaving a residual solid composed of $3NH_4NO_3(NH_4)_2SO_4$, NH_4Cl, and $NaNO_3.Na_2SO_4.H_2O$ until reaching 68% of RH. The daily DRH happens at 71.3 ± 4.9% and 67.1 ± 3.4% for $PM_{2.5}$ and $PM_{2.5-10}$, respectively, as shown in Figs. S4(b) and S4(c). In the OPC data analysis, an RH threshold of ≤ 50% was applied to determine the sensitivity. At this threshold, $PM_{2.5}$ particles have not yet deliquesced, and $PM_{2.5-10}$ shows minimal volume growth, indicating the applicability of the selected RH threshold for sensitivity calculation. A DRH threshold of 70% was applied to ensure sufficient data points for κ calculation but slightly lower than the DRH of $PM_{2.5}$.

To assess the potential bias associated with the selected DRH threshold, Fig. S6 shows the HGF of mean soluble composition as a function of RH estimated using E-AIM. With Eq. (2) (without the Kelvin effect term) and the assumption of volume additivity between particle and uptaken water, κ derived using 70% and 75% thresholds show less than 1% difference for both $PM_{2.5}$ and $PM_{2.5-10}$ compositions, but 13% and 6% less than that estimated from the composition calculation (Eq. (5)) for $PM_{2.5}$ and $PM_{2.5-10}$, respectively. As the selected DRH threshold decreases, the derived κ decreases slightly due to the interference of

adding data points with incompletely dissociated composition to the fitting analysis. However, the temporal composition variation in the applied OPC dataset (~16 days of observation) might lead to a higher variation (Fig. S7), making the κ deviation due to the applied DRH threshold appear negligible in this study. Furthermore, the lower derived κ for E-AIM compared to the composition estimation is likely due to the applied individual κ values in composition estimation being based on CCN activation measurement, which was reported to be 10% to 17% higher than that derived from the growth factor analysis (Petters and Kreidenweis, 2007). During the particle growth process, the partial dissociation leads to RH-dependent van't Hoff factor, as noted by Petters and Kreidenweis (2007). Similar findings were reported by Kreidenweis et al. (2008) regarding the differences in derived water contents between the κ-Köhler equation and E-AIM to be within ±20% under the condition of approximately 85% RH, which might cause differences for κ evaluation. Overall, the differences in derived κ among methods are primarily due to the given hygroscopicity of chemical species, likely due to the fixed van't Hoff factor and the assumptions of volume additivity in the κ-Köhler equation.

3.4 Sensitivity of assumed parameters on derived hygroscopicity

For simplicity, κ was derived from OPC and BAM data without considering the Kelvin effect and under an assumed particle density. Neglecting the Kelvin effect may result in minor differences for particles larger than 100 nm under sub-saturated conditions (Pope et al., 2010; Topping et al., 2005; Crilley et al., 2018). To confirm the appropriateness, we assessed biases for particles at 0.1 and 1 μm without considering the Kelvin effect, as shown in Fig. S8. For particles with a κ value of 0.3 under RH ranging from 70% to 95%, the deviation of κ due to neglecting the Kelvin effect is -10% for 0.1 μm particles and -1% for 1 μm particles, decreasing with particle diameter. The particle diameter is overestimated under the same RH conditions because the positive Kelvin effect is ignored. To compensate for the deficiency in saturation, the balanced particle diameter needs to be larger with a more significant solute effect. However, the average mass-weighted mean diameter for $PM_{2.5}$ is about 1.3 μm. Therefore, neglecting Kelvin effect in our analysis has limited influence on the derived κ.

Furthermore, the derived κ from OPC data (using Eq. (3)) and IC data (using Eq. (5)) are notably influenced by the assumed particle density. Assuming that the undetermined composition mainly consists of secondary organic species with a density of 1.2 g cm^{-3}, within the reported densities ranging from 0.9 to 1.6 g cm^{-3} depending on the formation process (Malloy et al., 2009; Kostenidou et al., 2007; Zelenyuk et al., 2008), along with the properties of analyzed soluble chemical species summarized in Table S2, the calculated densities are 1.42 ± 0.03 and 1.34 ± 0.05 g cm^{-3} for $PM_{2.5}$ and $PM_{2.5-10}$, respectively (Fig. S9). These calculated densities are about 15% and 10% higher than the assumed fixed density (1.2 g cm^{-3}) for $PM_{2.5}$ and $PM_{2.5-10}$, respectively. Consequently, the derived κ from OPC data increases by approximately 17% for $PM_{2.5}$ and 9% for $PM_{2.5-10}$, respectively, while the derived κ from IC data is proportional to density (i.e., 15% and 10% for $PM_{2.5}$ and $PM_{2.5-10}$, respectively) as shown in Fig. 4(b). This influence is particularly noticeable for components with a high portion of higher-density species, such as black carbon (a non-hygroscopic species with κ~0) having a high density of about 1.8 g cm^{-3} (Park et al., 2004; Shiraiwa et al., 2008). Despite the potential uncertainties associated with particle density, the derived κ exhibits consistency between the OPC and IC analyses.

4 Conclusion

In this study, we evaluated the performances of home-built Air Quality Box (AQB) systems equipped with low-cost sensors and focused on the ambient variability of particulate matter (PM) concentrations to derive the hygroscopicity of PM and the conversion to dry particle concentrations. The AQB systems revealed their effectiveness in capturing meteorological parameters and most pollutant concentrations with high correlations ($r \geq 0.96$) for temperature, relative humidity, CO, and Ox ($O_3 + NO_2$) and moderate correlations ($r \geq 0.48$) for NOx and PM, as compared to TW-EPA data. In the PM analysis, PM_{10} was divided into $PM_{2.5}$ and $PM_{2.5\text{-}10}$ to account for compositional heterogeneity among different particle sizes. Comparing the OPC-monitored ambient PM data and the BAM data (for dry particles) at RH ≤ 50%, the derived sensitivity coefficients (α) for $PM_{2.5\text{-}10}$ (10.58 - 12.37) were higher than those for $PM_{2.5}$ (1.26 - 1.44) likely due to the significant sensitivity variation in the OPC over time. By considering hygroscopicity with the κ-Köhler equation and assuming a constant composition density for sensitivity-corrected OPC data, the derived dry particle mass concentrations show improved consistency with BAM data compared to the simple linear regression approach. The derived κ values range from 0.15 to 0.29 for $PM_{2.5}$ and 0.05 to 0.13 for $PM_{2.5\text{-}10}$, consistent with those from IC soluble composition analysis (0.14 to 0.27 for $PM_{2.5}$ and 0.06 to 0.21 for $PM_{2.5\text{-}10}$) and primarily influenced by the proportion of soluble components, ~53% in $PM_{2.5}$ and ~30% in $PM_{2.5\text{-}10}$. The sensitivity analysis of various parameters showed that the effects of chosen deliquescence relative humidity (DRH) thresholds and Kelvin effect have a minor impact on κ values (less than 1%). Conversely, recalculating particle densities for $PM_{2.5}$ (1.42 ± 0.03 g cm^{-3}) and $PM_{2.5\text{-}10}$ (1.34 ± 0.07 g cm^{-3}) led to higher κ values by approximately 17% and 9%, respectively, compared to the results assuming a density of 1.2 g cm^{-3}. Overall, the AQB systems are potentially helpful in understanding the temporal and spatial variability of air quality by effectively monitoring pollutant concentrations and providing the capability for hygroscopicity derivation. This study also emphasizes the need for careful consideration of uncertainties and calibration techniques to interpret low-cost sensor data accurately in atmospheric research.

Code & Data availability

The code is not publicly accessible, but readers can contact HM Hung (hmhung@ntu.edu.tw) for more information. The observation data for AQBs and TW-EPA, the E-AIM model output, and the hygroscopicity deriving result used in this study can be accessed online at https://github.com/NTUACLab/Wei-Chieh.

Author contributions

WC Huang carried out the calibration campaign, analyzed data, and prepared the manuscript draft. HM Hung supervised the project, which included data discussion and manuscript editing. CW Chu and WC Hwang designed the home-built AQB system

and did database generation. SCC Lung supervised the field study in 2013 and conducted the aerosol composition analysis in 2021.

Competing interests

The authors declare that they have no conflict of interest.

Acknowledgments

We appreciate Taiwan EPA for providing the minute-averaged data of meteorological parameters and chemical species for calibration and comparison and Dr. Shih-Chieh Hsu at Research Center for Environmental Changes, Academia Sinica, Taipei, for composition data of $PM_{2.5}$ and PM_{10} in Kaohsiung (2013). This study was supported by the National Science and Technology Council in Taiwan (111-2111-M-002-009 and 112-2111-M-002-014).

References

Andreae, M. O. and Rosenfeld, D.: Aerosol–cloud–precipitation interactions. Part 1. The nature and sources of cloud-active aerosols, Earth-Sci. Rev., 89, 13-41, https://doi.org/10.1016/j.earscirev.2008.03.001, 2008.

Bian, Y. X., Zhao, C. S., Ma, N., Chen, J., and Xu, W. Y.: A study of aerosol liquid water content based on hygroscopicity measurements at high relative humidity in the North China Plain, Atmos. Chem. Phys., 14, 6417-6426, 10.5194/acp-14-6417-2014, 2014.

Brook, R. D., Rajagopalan, S., Pope, C. A., Brook, J. R., Bhatnagar, A., Diez-Roux, A. V., Holguin, F., Hong, Y., Luepker, R. V., Mittleman, M. A., Peters, A., Siscovick, D., Smith, S. C., Whitsel, L., and Kaufman, J. D.: Particulate Matter Air Pollution and Cardiovascular Disease, Circulation, 121, 2331-2378, 10.1161/CIR.0b013e3181dbece1, 2010.

Castell, N., Dauge, F. R., Schneider, P., Vogt, M., Lerner, U., Fishbain, B., Broday, D., and Bartonova, A.: Can commercial low-cost sensor platforms contribute to air quality monitoring and exposure estimates?, Environ. Int., 99, 293-302, 10.1016/j.envint.2016.12.007, 2017.

Chan, M. N. and Chan, C. K.: Mass transfer effects in hygroscopic measurements of aerosol particles, Atmos. Chem. Phys., 5, 2703-2712, 10.5194/acp-5-2703-2005, 2005.

Chen, C. L., Chen, T. Y., Hung, H. M., Tsai, P. W., Chou, C. C. K., and Chen, W. N.: The influence of upslope fog on hygroscopicity and chemical composition of aerosols at a forest site in Taiwan, Atmos. Environ., 246, 10.1016/j.atmosenv.2020.118150, 2021.

Chen, S. Y., Chan, C. C., and Su, T. C.: Particulate and gaseous pollutants on inflammation, thrombosis, and autonomic imbalance in subjects at risk for cardiovascular disease, Environ. Pollut., 223, 403-408, 10.1016/j.envpol.2017.01.037, 2017.

Clegg, S. L., Brimblecombe, P., and Wexler, A. S.: Thermodynamic model of the system H^+-NH_4^+-Na^+-SO_4^{2-}-NO_3^--Cl^--H_2O at 298.15 K, J. Phys. Chem. A, 102, 2155-2171, 10.1021/jp973043j, 1998.

Concas, F., Mineraud, J., Lagerspetz, E., Varjonen, S., Liu, X. L., Puolamaki, K., Nurmi, P., and Tarkoma, S.: Low-Cost Outdoor Air Quality Monitoring and Sensor Calibration: A Survey and Critical Analysis, ACM Trans. Sens. Netw., 17, 10.1145/3446005, 2021.

Crilley, L. R., Shaw, M., Pound, R., Kramer, L. J., Price, R., Young, S., Lewis, A. C., and Pope, F. D.: Evaluation of a low-cost optical particle counter (Alphasense OPC-N2) for ambient air monitoring, Atmos. Meas. Tech., 11, 709-720, 10.5194/amt-11-709-2018, 2018.

Dacunto, P. J., Klepeis, N. E., Cheng, K.-C., Acevedo-Bolton, V., Jiang, R.-T., Repace, J. L., Ott, W. R., and Hildemann, L. M.: Determining $PM_{2.5}$ calibration curves for a low-cost particle monitor: common indoor residential aerosols, Environ. Sci.: Process. Impacts, 17, 1959-1966, 10.1039/c5em00365b, 2015.

Demanega, I., Mujan, I., Singer, B. C., Andelkovic, A. S., Babich, F., and Licina, D.: Performance assessment of low-cost environmental monitors and single sensors under variable indoor air quality and thermal conditions, Build. Environ., 187, 10.1016/j.buildenv.2020.107415, 2021.

Di Antonio, A., Popoola, O. A. M., Ouyang, B., Saffell, J., and Jones, R. L.: Developing a Relative Humidity Correction for Low-Cost Sensors Measuring Ambient Particulate Matter, Sensors, 18, 2790, 2018.

Formenti, P., Di Biagio, C., Huang, Y., Kok, J., Mallet, M. D., Boulanger, D., and Cazaunau, M.: Look−up tables resolved by complex refractive index to correct particle sizes measured by common research−grade optical particle counters, Atmos. Meas. Tech. Discuss., 2021, 1-30, 10.5194/amt-2021-403, 2021.

Gillooly, S. E., Zhou, Y., Vallarino, J., Chu, M. T., Michanowicz, D. R., Levy, J. I., and Adamkiewicz, G.: Development of an in-home, real-time air pollutant sensor platform and implications for community use, Environ. Pollut., 244, 440-450, https://doi.org/10.1016/j.envpol.2018.10.064, 2019.

Glockler, G.: The ionization potential of methane, Journal of the American Chemical Society, 48, 2021-2026, 10.1021/ja01419a002, 1926.

Hagan, D. H. and Kroll, J. H.: Assessing the accuracy of low-cost optical particle sensors using a physics-based approach, Atmospheric Measurement Techniques, 13, 6343-6355, 10.5194/amt-13-6343-2020, 2020.

Hamanaka, R. B. and Mutlu, G. M.: Particulate Matter Air Pollution: Effects on the Cardiovascular System, Front. Endocrinol., 9, 10.3389/fendo.2018.00680, 2018.

Hering, S. and Cass, G.: The Magnitude of Bias in the Measurement of PM_{25} Arising from Volatilization of Particulate Nitrate from Teflon Filters, J. Air Waste Manag. Assoc., 49, 725-733, 10.1080/10473289.1999.10463843, 1999.

Heus, T., van Heerwaarden, C. C., Jonker, H. J. J., Siebesma, A. P., Axelsen, S., van den Dries, K., Geoffroy, O., Moene, A. F., Pino, D., de Roode, S. R., and de Arellano, J. V. G.: Formulation of the Dutch Atmospheric Large-Eddy Simulation (DALES) and overview of its applications, Geosci. Model Dev., 3, 415-444, 10.5194/gmd-3-415-2010, 2010.

Hung, H.-M., Hsu, C.-H., Lin, W.-T., and Chen, Y.-Q.: A case study of single hygroscopicity parameter and its link to the functional groups and phase transition for urban aerosols in Taipei City, Atmos. Environ., 132, 240-248, https://doi.org/10.1016/j.atmosenv.2016.03.008, 2016.

Kaliszewski, M., Włodarski, M., Młyńczak, J., and Kopczyński, K.: Comparison of Low-Cost Particulate Matter Sensors for Indoor Air Monitoring during COVID-19 Lockdown, Sensors (Basel), 20, 10.3390/s20247290, 2020.

Karagulian, F., Barbiere, M., Kotsev, A., Spinelle, L., Gerboles, M., Lagler, F., Redon, N., Crunaire, S., and Borowiak, A.: Review of the Performance of Low-Cost Sensors for Air Quality Monitoring, Atmos., 10, 10.3390/atmos10090506, 2019.

Kostenidou, E., Pathak, R. K., and Pandis, S. N.: An algorithm for the calculation of secondary organic aerosol density combining AMS and SMPS data, Aerosol Sci. Technol., 41, 1002-1010, 10.1080/02786820701666270, 2007.

Kreidenweis, S. M., Petters, M. D., and DeMott, P. J.: Single-parameter estimates of aerosol water content, Environ. Res. Lett., 3, 035002, 10.1088/1748-9326/3/3/035002, 2008.

Li, J., Liu, W. Y., Castarede, D., Gu, W. J., Li, L. J., Ohigashi, T., Zhang, G. Q., Tang, M. J., Thomson, E. S., Hallquist, M., Wang, S., and Kong, X. R.: Hygroscopicity and Ice Nucleation Properties of Dust/Salt Mixtures Originating from the Source of East Asian Dust Storms, Front. Environ. Sci., 10, 10.3389/fenvs.2022.897127, 2022.

Lohmann, U. and Feichter, J.: Global indirect aerosol effects: a review, Atmos. Chem. Phys., 5, 715-737, 10.5194/acp-5-715-2005, 2005.

Luo, Q., Hong, J., Xu, H., Han, S., Tan, H., Wang, Q., Tao, J., Ma, N., Cheng, Y., and Su, H.: Hygroscopicity of amino acids and their effect on the water uptake of ammonium sulfate in the mixed aerosol particles, Sci. Total Environ., 734, 139318, https://doi.org/10.1016/j.scitotenv.2020.139318, 2020.

Malloy, Q. G. J., Nakao, S., Qi, L., Austin, R., Stothers, C., Hagino, H., and Cocker, D. R.: Real-Time Aerosol Density Determination Utilizing a Modified Scanning Mobility Particle Sizer—Aerosol Particle Mass Analyzer System, Aerosol Sci. Technol., 43, 673-678, 10.1080/02786820902832960, 2009.

Mead, M. I., Popoola, O. A. M., Stewart, G. B., Landshoff, P., Calleja, M., Hayes, M., Baldovi, J. J., McLeod, M. W., Hodgson, T. F., Dicks, J., Lewis, A., Cohen, J., Baron, R., Saffell, J. R., and Jones, R. L.: The use of electrochemical sensors for

monitoring urban air quality in low-cost, high-density networks, Atmos. Environ., 70, 186-203, 10.1016/j.atmosenv.2012.11.060, 2013.
Pöschl, U., Martin, S. T., Sinha, B., Chen, Q., Gunthe, S. S., Huffman, J. A., Borrmann, S., Farmer, D. K., Garland, R. M., Helas, G., Jimenez, J. L., King, S. M., Manzi, A., Mikhailov, E., Pauliquevis, T., Petters, M. D., Prenni, A. J., Roldin, P., Rose, D., Schneider, J., Su, H., Zorn, S. R., Artaxo, P., and Andreae, M. O.: Rainforest aerosols as biogenic nuclei of clouds and precipitation in the Amazon, N Y Sci J, 329, 1513-1516, 10.1126/science.1191056, 2010.
Park, K., Kittelson, D. B., Zachariah, M. R., and McMurry, P. H.: Measurement of Inherent Material Density of Nanoparticle Agglomerates, J. Nanoparticle Res., 6, 267-272, 10.1023/B:NANO.0000034657.71309.e6, 2004.
Petters, M. D. and Kreidenweis, S. M.: A single parameter representation of hygroscopic growth and cloud condensation nucleus activity, Atmos. Chem. Phys., 7, 1961-1971, 10.5194/acp-7-1961-2007, 2007.
Pope, F. D., Dennis-Smither, B. J., Griffiths, P. T., Clegg, S. L., and Cox, R. A.: Studies of Single Aerosol Particles Containing Malonic Acid, Glutaric Acid, and Their Mixtures with Sodium Chloride. I. Hygroscopic Growth, J. Phys. Chem. A, 114, 5335-5341, 10.1021/jp100059k, 2010.
Pringle, K. J., Tost, H., Pozzer, A., Pöschl, U., and Lelieveld, J.: Global distribution of the effective aerosol hygroscopicity parameter for CCN activation, Atmos. Chem. Phys., 10, 5241-5255, 10.5194/acp-10-5241-2010, 2010.
Rosenfeld, D., Andreae, M. O., Asmi, A., Chin, M., de Leeuw, G., Donovan, D. P., Kahn, R., Kinne, S., Kivekas, N., Kulmala, M., Lau, W., Schmidt, K. S., Suni, T., Wagner, T., Wild, M., and Quaas, J.: Global observations of aerosol-cloud-precipitation-climate interactions, Rev. Geophys., 52, 750-808, 10.1002/2013rg000441, 2014.
Salvador, C. M. and Chou, C. C. K.: Analysis of semi-volatile materials (SVM) in fine particulate matter, Atmos. Environ., 95, 288-295, https://doi.org/10.1016/j.atmosenv.2014.06.046, 2014.
Samad, A., Mimiaga, F. E. M., Laquai, B., and Vogt, U.: Investigating a Low-Cost Dryer Designed for Low-Cost PM Sensors Measuring Ambient Air Quality, Sensors, 21, 10.3390/s21030804, 2021.
Shiraiwa, M., Kondo, Y., Moteki, N., Takegawa, N., Sahu, L. K., Takami, A., Hatakeyama, S., Yonemura, S., and Blake, D. R.: Radiative impact of mixing state of black carbon aerosol in Asian outflow, J. Geophys. Res. D: Atmos., 113, https://doi.org/10.1029/2008JD010546, 2008.
Sá, J. P., Alvim-Ferraz, M. C. M., Martins, F. G., and Sousa, S. I. V.: Application of the low-cost sensing technology for indoor air quality monitoring: A review, Environ. Technol. Innov., 28, 102551, https://doi.org/10.1016/j.eti.2022.102551, 2022.
Tang, M. J., Zhang, H. H., Gu, W. J., Gao, J., Jian, X., Shi, G. L., Zhu, B. Q., Xie, L. H., Guo, L. Y., Gao, X. Y., Wang, Z., Zhang, G. H., and Wang, X. M.: Hygroscopic Properties of Saline Mineral Dust From Different Regions in China: Geographical Variations, Compositional Dependence, and Atmospheric Implications, J. Geophys. Res. D: Atmos., 124, 10844-10857, 10.1029/2019jd031128, 2019.
Topping, D. O., McFiggans, G. B., and Coe, H.: A curved multi-component aerosol hygroscopicity model framework: Part 1 – Inorganic compounds, Atmos. Chem. Phys., 5, 1205-1222, 10.5194/acp-5-1205-2005, 2005.
Venkatraman Jagatha, J., Klausnitzer, A., Chacón-Mateos, M., Laquai, B., Nieuwkoop, E., van der Mark, P., Vogt, U., and Schneider, C.: Calibration Method for Particulate Matter Low-Cost Sensors Used in Ambient Air Quality Monitoring and Research, Sensors, 21, 3960, 2021.
Wu, C. F., Kuo, I. C., Su, T. C., Li, Y. R., Lin, L. Y., Chan, C. C., and Hsu, S. C.: Effects of Personal Exposure to Particulate Matter and Ozone on Arterial Stiffness and Heart Rate Variability in Healthy Adults, Am. J. Epidemiol., 171, 1299-1309, 10.1093/aje/kwq060, 2010.
Zelenyuk, A., Yang, J., Song, C., Zaveri, R. A., and Imre, D.: A new real-time method for determining particles' sphericity and density: application to secondary organic aerosol formed by ozonolysis of alpha-pinene, Environ. Sci. Technol., 42, 8033-8038, 10.1021/es8013562, 2008.

Tables

Table 1: The sensitivity coefficients and the hygroscopicity for $PM_{2.5}$, PM_{10} and $PM_{2.5-10}$.

	Sensitivity coefficient (α)		Hygroscopicity (κ)			
	AQB #1	AQB #2*	AQB #1	AQB #2	IC (species)	IC (E-AIM)
$PM_{2.5}$	1.26 ± 0.16	1.44 ± 0.20	0.18 – 0.29	0.15– 0.24	0.14 – 0.27	0.14 – 0.26
PM_{10}	2.02 ± 0.34	2.20 ± 0.38	0.20 – 0.39	0.18 – 0.30		
$PM_{10}^{\#}$	$\alpha_{2.5}$, $\alpha_{2.5-10}$	$\alpha_{2.5}$, $\alpha_{2.5-10}$	0.13 – 0.23	0.11 – 0.26		
$PM_{2.5-10}$	12.37 ± 1.33	10.58 ± 2.90	0.07 – 0.13	0.05 – 0.09	0.06 – 0.21	0.08 – 0.21

$^{\#}$ the hygroscopicity derived using different sensitivity coefficients for different size ranges. $\alpha_{2.5}$ and $\alpha_{2.5-10}$ are sensitivity coefficients for $PM_{2.5}$ and $PM_{2.5-10}$, respectively. More details are provided in the description of the supplementary material.

*** the sensitivity of AQB #2 presents the value in the period of sampling flow rates at 3.6-4.2 LPM**

Table 2: Performance metrics of different calibration methods for $PM_{2.5}$, $PM_{2.5-10}$, and PM_{10}.

	$PM_{2.5}$			$PM_{2.5-10}$			PM_{10}			
	RH≤50% only[a]	All data (no κ)	All data (κ = 0.29)	RH≤50% only[a]	All data (no κ)	All data (κ = 0.09)	RH≤50% only[a]	All data (no κ)	All data (κ = 0.36)	($PM_{2.5}$+ $PM_{2.5-10}$) [c]
applied α	1.26 ± 0.16	1.04	1.40	12.37 ± 1.33	10.77	13.16	2.02 ± 0.34	1.69	2.36	—
MAPE (%)	21.3 (12.8)	48.8	24.8	15.9 (11.5)	37.9	31.8	32.8 (18.5)	62.5	29.2	18.2
RMSE (μg cm^{-3})	20.5 (3.7)	29.1	11.3	4.9 (2.8)	9.4	9.1	42.6 (10.3)	54.7	26.9	15.9
R^2 [b]	-0.55 (0.51)	-3.49	0.32	0.31 (0.78)	0.57	0.59	-4.18 (-0.58)	-4.74	-0.38	0.51

[a] Only for data points at RH ≤50%. The value in parentheses is the performance result without two significant outliers shown in Fig. 3

[b] Coefficient of determination (R^2) is calculated as the proportion of variation in the calibrated dry mass concentration.

[c] The combination of calibrated data from $PM_{2.5}$ All data (κ= 0.29) and $PM_{2.5-10}$ All data (κ= 0.09).

Table 3. The total mass concentration, the major water-soluble composition and concentration (mean value and standard deviation in μg m^{-3}) of winter $PM_{2.5}$ and $PM_{2.5-10}$ in Kaohsiung by ion chromatography. (others presented the insoluble composition)

Ion species	Total	Na^+	Mg^{2+}	K^+	Ca^{2+}	NH_4^+	Cl^-	SO_4^{2-}	NO_3^-	others
$PM_{2.5}$	67.0 ± 19.2	0.31 ± 0.14	0.06 ± 0.02	0.45 ± 0.14	0.08 ± 0.04	8.24 ± 2.68	1.21 ± 0.91	13.63 ± 4.72	11.89 ± 4.88	31.1 ± 8.0
$PM_{2.5-10}$	36.8 ± 7.64	1.50 ± 0.52	0.21 ± 0.06	0.04 ± 0.02	0.74 ± 0.25	1.07 ± 0.69	1.28 ± 0.69	1.87 ± 1.12	4.35 ± 1.41	25.7 ± 6.4

Figures

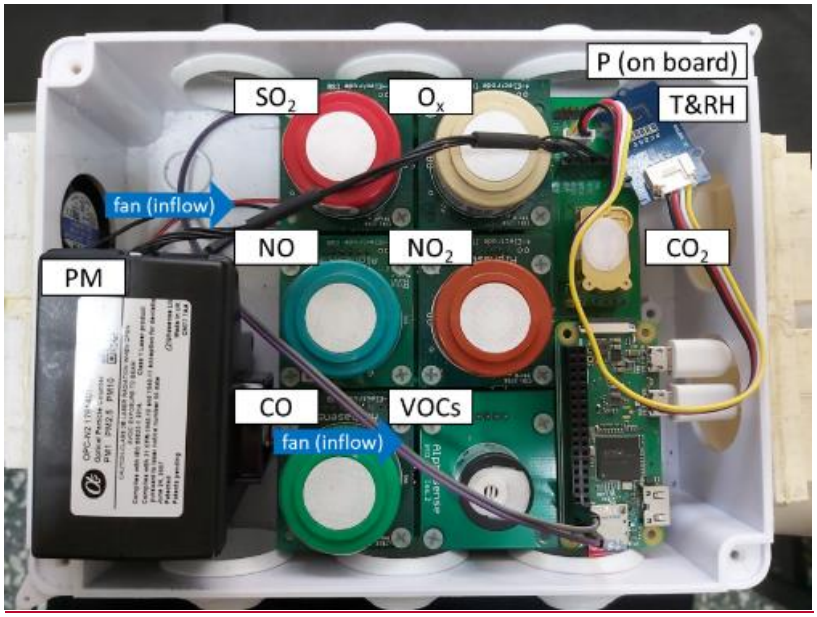

Figure 1: The design of the AQB system.

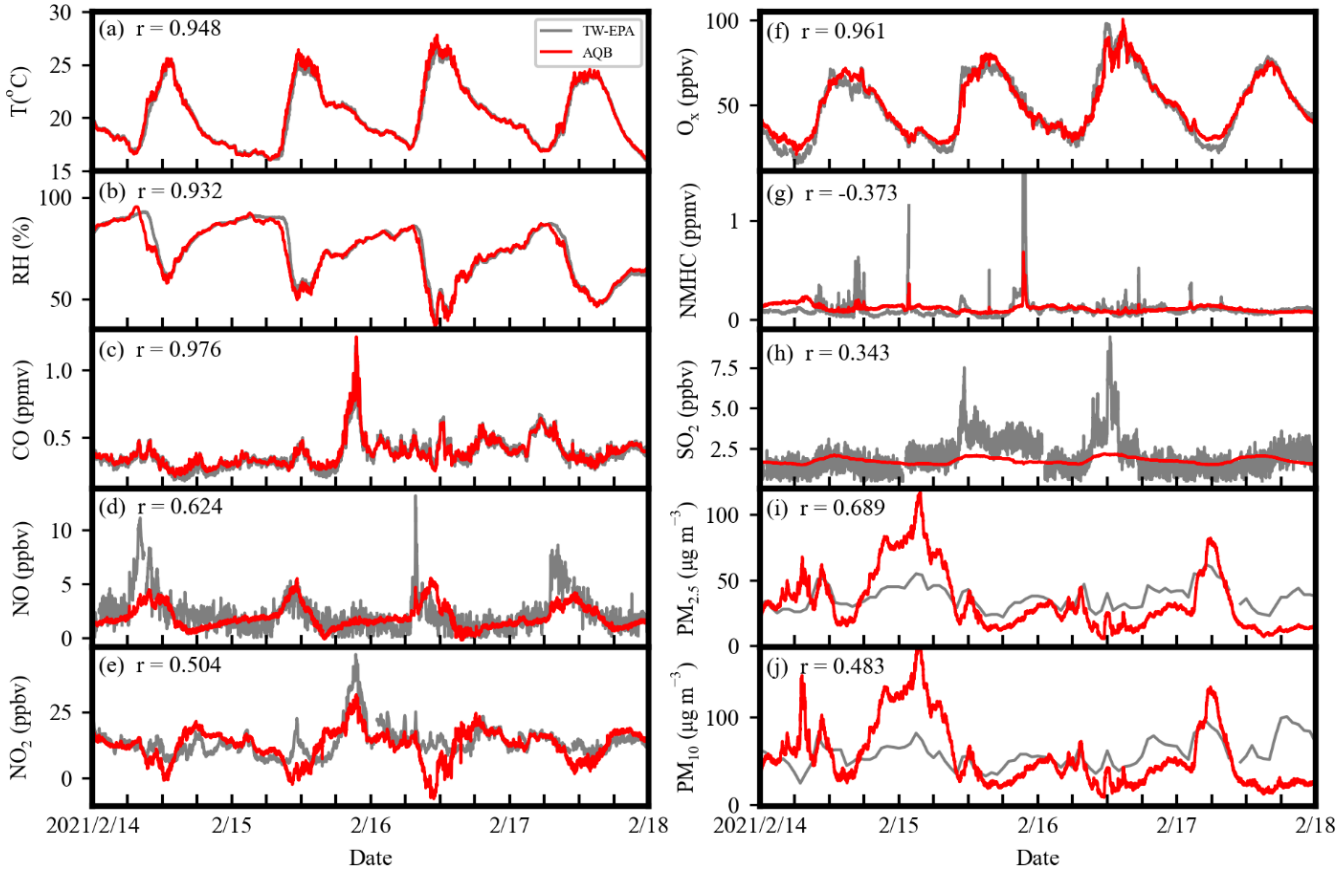

515

Figure 2: The temporal profiles of calibrated AQB data (red lines) and the TW-EPA measurement (grey lines) for (a) temperature, (b) relative humidity, (c) CO, (d) NO, (e) NO_2, (f) Ox (≡ NO_2 + O_3), (g) Non-methane hydrocarbon, (h) SO_2, (i) $PM_{2.5}$, and (j) PM_{10} during the period of 14 – 17 February 2021 (4 of 16 days in period). All the species were calibrated using linear regression.

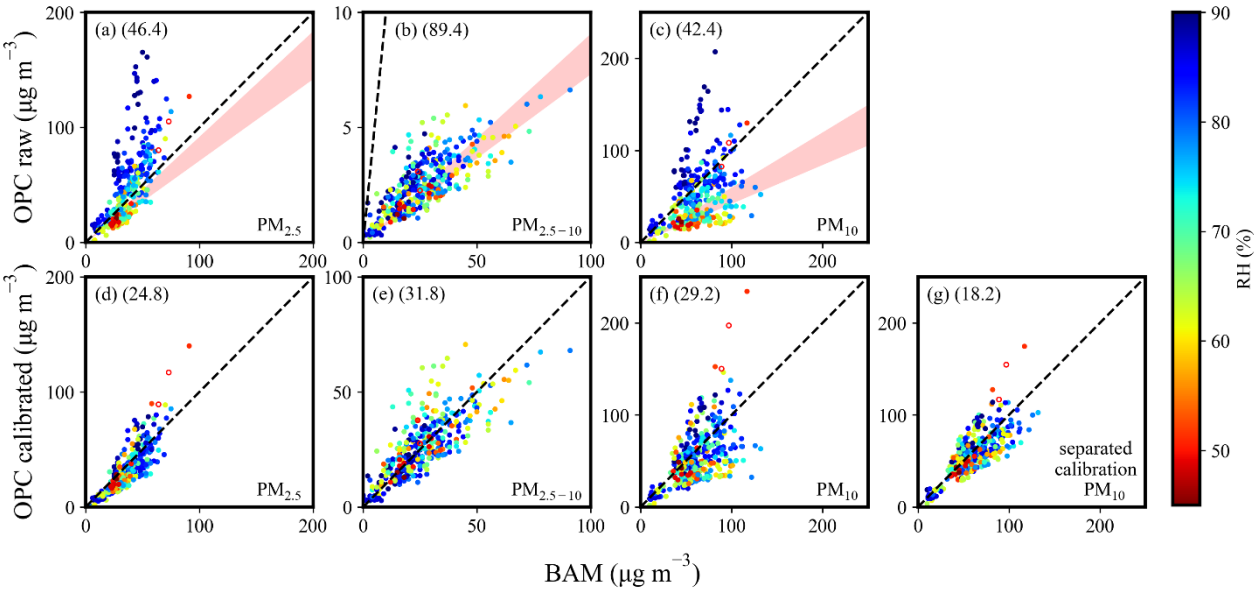

Figure 3: The correlation of mass concentration between BAM and OPC in AQB #1 (raw data or calibrated data): (a, d) $PM_{2.5}$, (b, e) $PM_{2.5\text{-}10}$, (c, f) PM_{10}, and (f) separated calibration PM_{10}, respectively. (a-c) are the raw data, while (d-g) are the calibrated data. The marker color corresponds to relative humidity. The hollow points are the two significant outliers under conditions of RH ≤ 50%. The shaded region represents the data associated with the sensitivity coefficient ("α"). The value in parentheses is the MAPE in percentage.

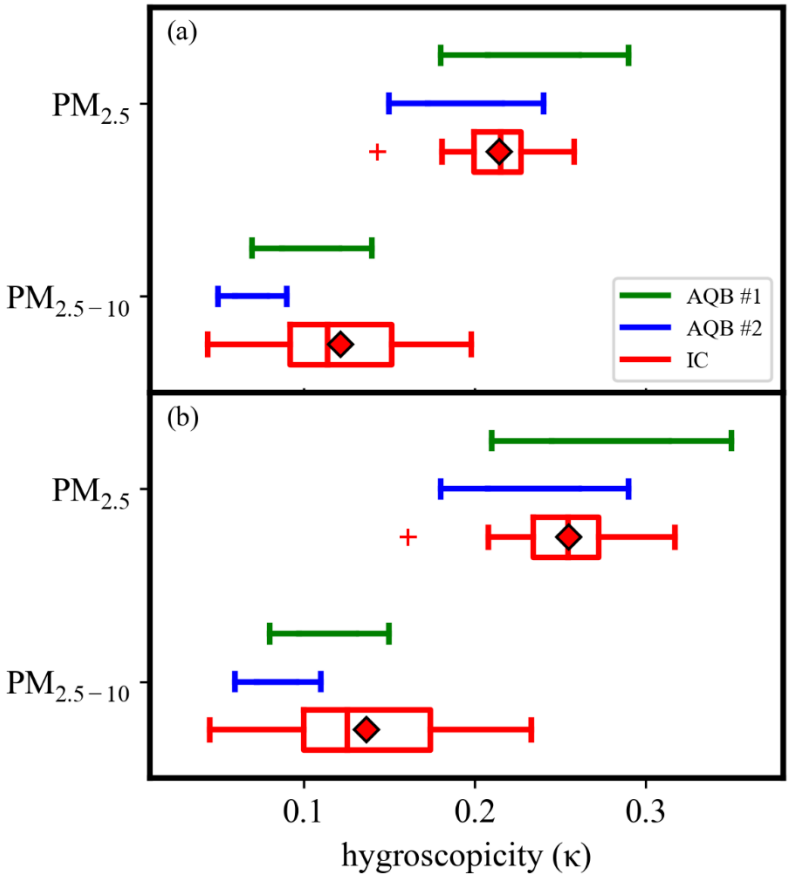

Figure 4: The hygroscopicities of $PM_{2.5}$ and $PM_{2.5-10}$ derived based on data from OPCs and ion chromatography with the assumption particle density of (a) 1.2 g cm^{-3} and (b) 1.42 ± 0.03 and 1.34 ± 0.07 g cm^{-3} for $PM_{2.5}$ and $PM_{2.5-10}$, respectively, based on analyzed composition. The average value is shown as a red diamond.

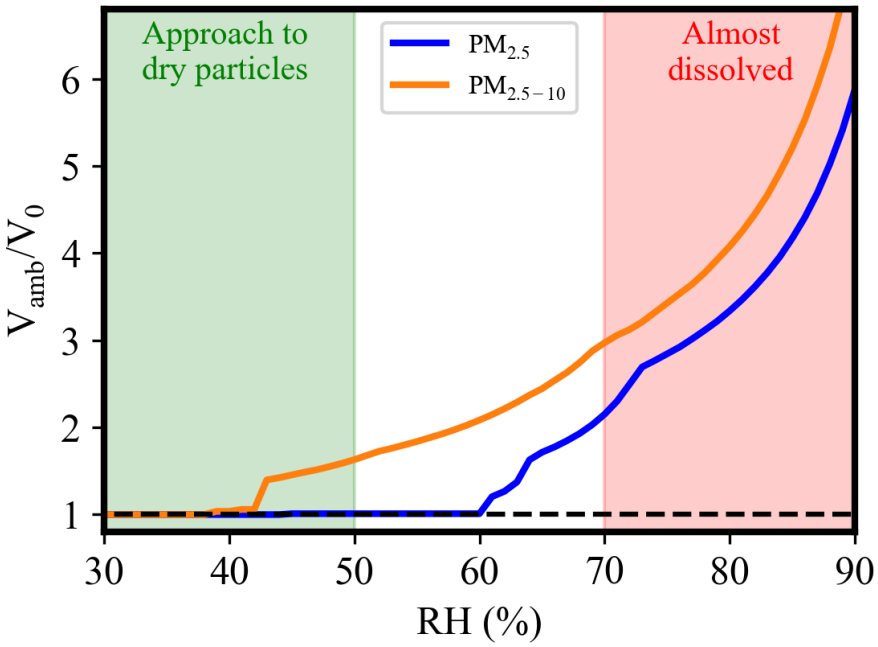

Figure 5: The volume ratio of a given soluble composition as a function of RH under thermodynamic equilibrium calculated using E-AIM at 298.15 K. (composition is the averaged IC data with a molarity ratio of Na^+:NH_4^+:Cl^-:SO_4^{2-}:NO_3^- as 7:229:0:71:94 for $PM_{2.5}$, and 65:59:16:19:70 for $PM_{2.5-10}$.)

Supplementary Material for

Deriving the hygroscopicity of ambient particles using low-cost optical particle counters

by

Wei-Chieh Huang[1], Hui-Ming Hung[1*], Ching-Wei Chu[1], Wei-Chun Hwang[1], and Shih-Chun Candice Lung[2]

Content of this file

Aerosol hygroscopicity derived using OPC and BAM data

The optical particle counter (OPC) (model: OPC-N2, Alphasense) provides digital outputs of PM_1, $PM_{2.5}$, PM_{10}, and optionally $PM_{4.25}$, along with histograms of the particle counts for 16 size bins ranging from 0.38 to 17 μm. This device is designed to monitor ambient aerosol concentrations without any drying system attached to the sampling inlet. In contrast, the Beta Attenuation Mass Monitor (BAM) (model: BAM1020, Met One Instrument) is designed to monitor dry particle mass concentrations of $PM_{2.5}$ and PM_{10}, using a heating device to ensure the sampling relative humidity (RH) remains below 50%. If the RH of the sampled air stream exceeds 50%, the inlet heater activates, reducing the RH to approximately 35% by warming the air stream downstream before reaching the filter tape. If the RH is below 50%, the heater remains inactive, not altering the sampling flow RH. The technical specifications for the OPC and BAM are summarized in Table S4.

To derive aerosol hygroscopicity (κ), the sensitivity coefficient of OPC was evaluated first using the data points at RH ≤ 50%, as described in Section 2.3 of the main content. Depending on the size range, $\alpha_{2.5}$, α_{10}, and $\alpha_{2.5\text{-}10}$ represent the sensitivity coefficient of OPC for $PM_{2.5}$, PM_{10}, and $PM_{2.5\text{-}10}$, respectively. For PM_{10}, a range of hygroscopicity of 0 to 1.2 was applied to Eq. (S1) to obtain $M_{d,derived,10}$ and evaluate the mean absolute percentage error (MAPE) between $M_{d,derived,10}$ and $M_{BAM,10}$. MAPE as a function of the applied hygroscopicity is plotted to determine the κ_{10} range, which has MAPE ≤ 1.1×the lowest MAPE, considering the uncertainty. A similar calculation is applied to $PM_{2.5}$, and $PM_{2.5\text{-}10}$ to derive $\kappa_{2.5}$ and $\kappa_{2.5\text{-}10}$ directly.

$$M_{d,derived,10} = \alpha_{10} \times M_{OPC,10} \times \left[\left(\frac{S\,\kappa_{10}}{1-S}\right) \times \frac{\rho_w}{\rho_d} + 1\right]^{-1} \quad \text{(S1)}$$

However, PM_{10}^{*} in Table 1 considers the size-dependent sensitivity with a mean hygroscopicity. κ_{10} is derived using the following equation:

$$M_{d,derived,10} = \left(\alpha_{2.5} \times M_{OPC,2.5} + \alpha_{2.5-10} \times M_{OPC,2.5-10}\right) \times \left[\left(\frac{S\,\kappa_{10}}{1-S}\right) \times \frac{\rho_w}{\rho_d} + 1\right]^{-1} \quad \text{(S2)}$$

The derived κ_{10} using Eq. (S2) ranges from 0.13 to 0.23, falling between κ values for $PM_{2.5}$ and $PM_{2.5\text{-}10}$, and is more reasonable than from Eq. (S1), as discussed in Section 3.2.2.

Table S1: Summary of the applied sensors in AQB and instruments at TW-EPA station.

	Sensors in AQB (Manufacturer)	Detection range, Detection resolution	Instruments at TW-EPA (Manufacturer)	Detection range, Detection resolution
T, RH	SHT31 (Seeed)	T: -40 – 125 ℃, 0.1 ℃ RH: 0 – 100%, 0.1%	083D (Met One Instruments)	T: -30–50 ℃, 0.1 ℃ RH: 0–100%, 0.04%
CO	CO-B4 (Alphasense)	0–1000 ppmv, in ppbv	APMA360 (Horiba)	0–100 ppmv, 0.02 ppmv
NO	NO-B4 (Alphasense)	0–20 ppmv, in ppbv	ML9841 (Horiba)	0–20 ppmv, 1 pptv
NO_2	NO2-B43F (Alphasense)	0–20 ppmv, in ppbv	ML9841 (Horiba)	0–20 ppmv, 1 pptv
O_3	OX-B431 for O_3+NO_2 (Alphasense)	0–20 ppmv, in ppbv	ML9810 (Ecotech)	0–20 ppmv, 1 pptv
SO_2	SO2-B4 (Alphasense)	0–100 ppmv, in ppbv	ML9850 (Ecotech)	0–20 ppmv, 1 pptv
VOC	PID-AH2 (Alphasense)	0–40 ppmv, in ppbv	APHA360 (Horiba)	0–100 ppmv, 0.022 ppmv
PM	OPC-N2 (Alphasense)	0.01–1500 μg m^{-3}, 0.1μg m^{-3}	BAM1020 (Met One Instruments)	0–10,000 μg m^{-3}, 0.1μg m^{-3}

Table S2: The hygroscopicity, molecular weight, and density of salts used in deriving hygroscopicity of mixtures.

salt	$(NH_4)_2SO_4$	$(NH_4)HSO_4$	NH_4NO_3	$NaNO_3$	NaCl
hygroscopicity	0.61[a]	0.80[c]	0.67[a]	0.88[a]	1.28[a]
molecular weight (g mol^{-1})	132	115	80	85	58.5
density (g cm^{-3})	1.70[b]	1.78[b]	1.72[b]	2.26	2.17

[a] hygroscopicity summarized in Petters and Kreidenweis (2007) as CCN derived hygroscopicity.

[b] density of chemical species reported by Xu et al. (2020).

[c] hygroscopicity calculated by Kim et al. (2021)

Table S3: The correlation coefficient (r) for measured parameters between two AQB systems and between AQB #1 and the TW-EPA Nanzi station

r	AQB #1 vs AQB #2	AQB #1 vs TW-EPA
T	0.958	0.948
RH	0.949	0.932
CO	0.995	0.976
NO	0.976	0.624
NO_2	0.944	0.504
Ox (NO_2+O_3)	0.979	0.961
VOC	0.675	-0.373
SO_2	0.973	0.343
$PM_{2.5}$	0.978	0.689
PM_{10}	0.967	0.483

Table S4: Technical specifications for OPC and BAM

	OPC	BAM
Manufacturer	Alphasense	Met One Instruments
Model	OPC-N2	BAM1020
Particle range (μm)	0.38 – 17	-
Bin number	16	-
Laser wavelength (nm)	658	-
Refractive index	1.5 + 0i	-
Setting particle density (g cm^{-3})	1.65	-
Max particle count rate (s^{-1})	10,000	-
Detection range (μg m^{-3})	0.01-1500 (for PM_{10})	0 – 10,000
Measurement resolution (μg m^{-3})	0.1	0.1
Sampling flow rate (LPM)	~5	16.67
Coincidence probability (% at 10^6 L^{-1})	0.84	-
Unit dimensions (L × D × H)	75 × 60 × 63.5 (mm)	36.2 × 43.2 × 46.7 (cm)
Weight	105 g	19 kg
Particle size designations (μm)	-	PM_{10}, $PM_{2.5}$, and $PM_{2.5-10}$
Filter tape	-	Continuous glass fiber filter

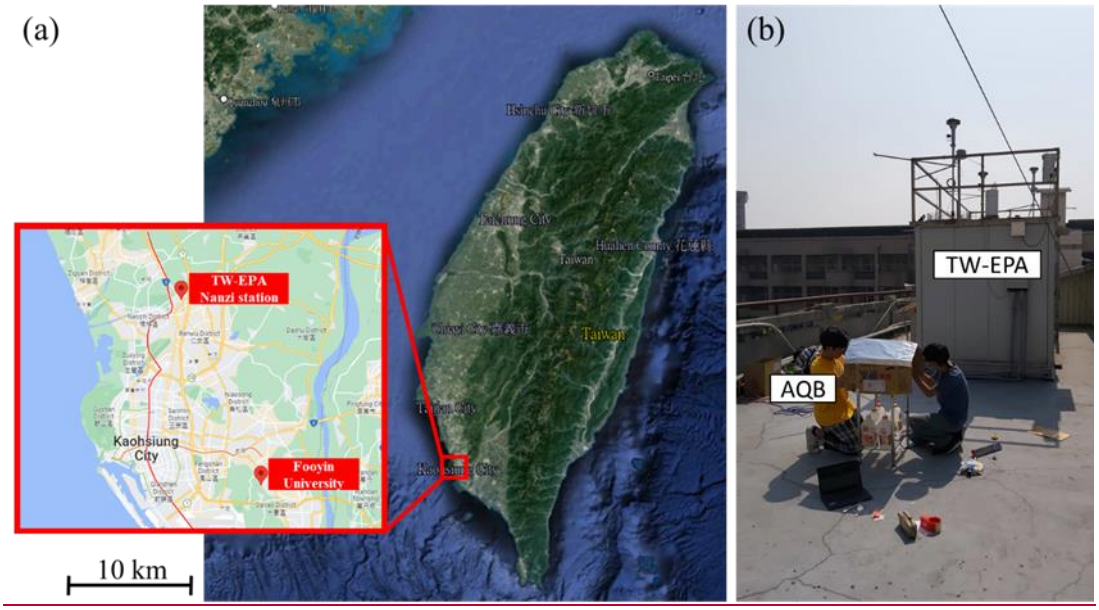

Figure S1. (a) Location of TW-EPA Nanzi station (AQB calibration campaign) site and Fooyin University (2013 sampling campaign). (from © Google Earth 2024 and © Google Maps 2024). (b) Photograph of the setup in AQB system operational state. AQB was located approximately 5 m horizontally and 2 m vertically from the sampling inlet of TW-EPA Nanzi station).

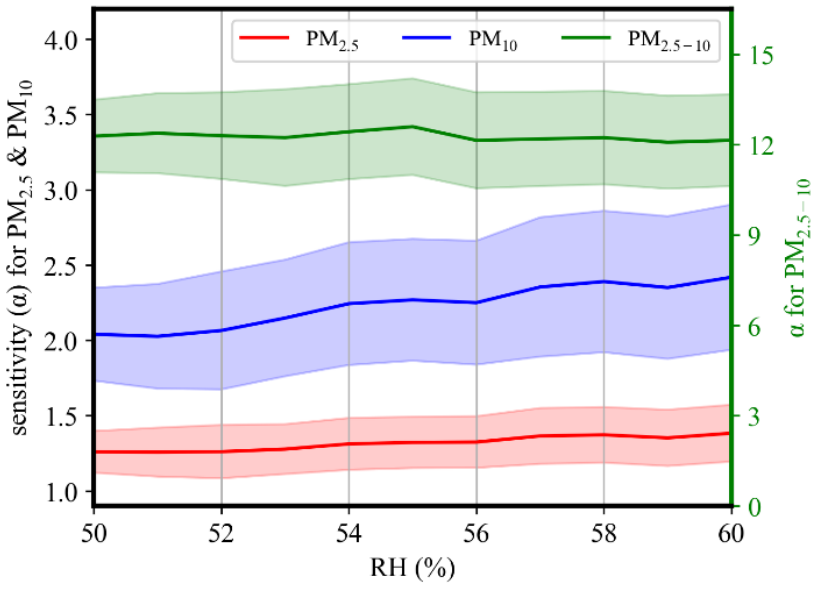

Figure S2: The determined sensitivity as a function of RH thresholds for $PM_{2.5}$ (red), PM_{10} (blue) and $PM_{2.5-10}$ (green). The shaded area represents the mean value ± 0.5σ

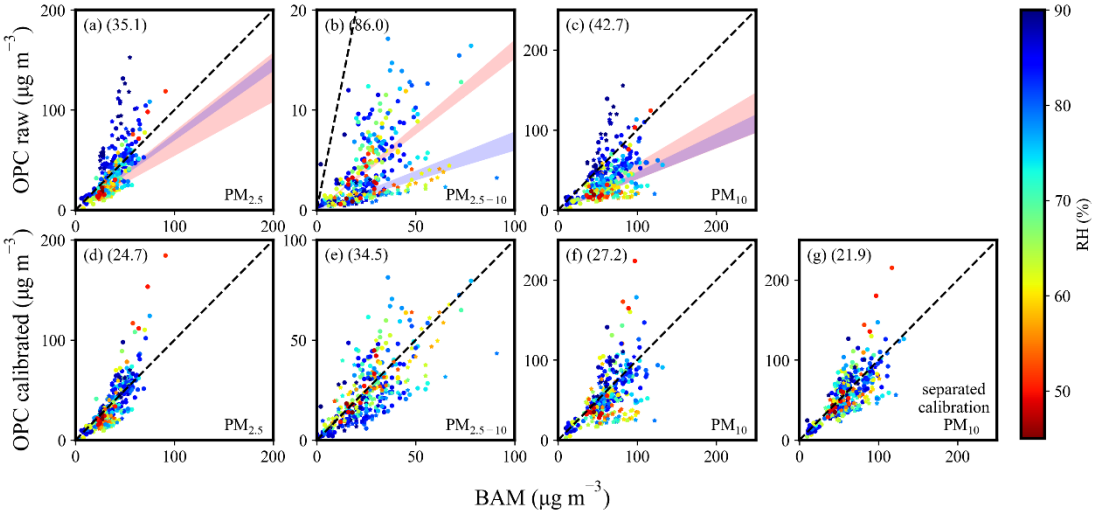

Figure S3: The correlation of mass concentration between BAM and OPC in AQB #2: (a, d) $PM_{2.5}$, (b, e) $PM_{2.5-10}$, (c, f) PM_{10}, and (g) separated calibration PM_{10}. (a-c) are the raw data, while (d-g) are the calibrated data. The marker color corresponds to RH. The shaded region represents the data associated with the sensitivity coefficient ("*α*"). The data show the first period (red paved/circle points) and the second period (purple paved/star points). The value in parentheses is the MAPE in percentage.

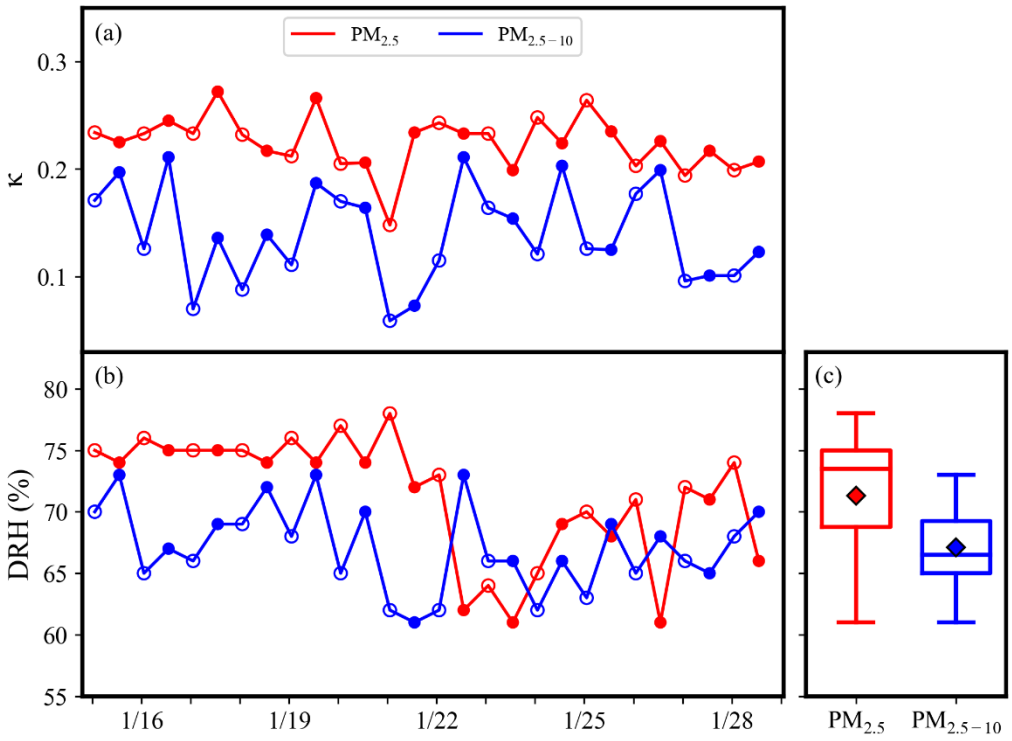

Figure S4: The temporal profiles of (a) derived κ from IC data, (b) DRH determined from E-AIM, and (c) DRH box-plot distribution for the 2013 winter campaign period. (hollow circle: daytime samples; solid circle: nighttime samples; diamond: mean value; outliers: < 1st quartile Q1-1.5 interquartile range (IQR) or > 3rd quartile Q3+1.5 IQR).

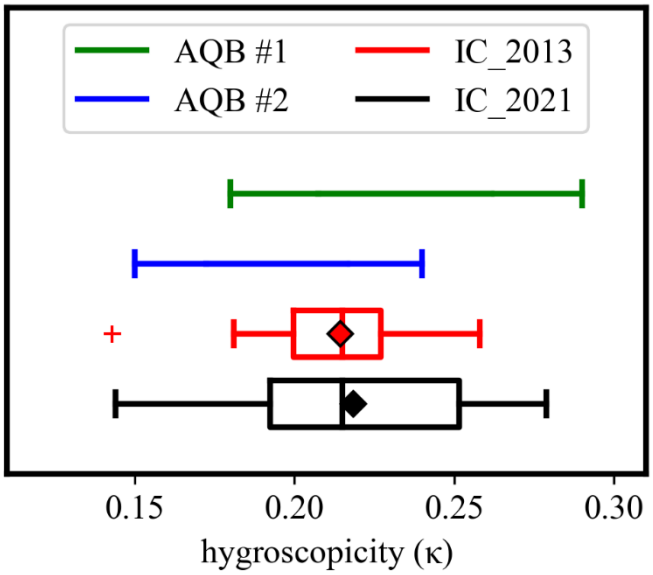

Figure S5: The hygroscopicity of $PM_{2.5}$ derived from OPC and IC data with an assumed particle density of 1.2 g cm^{-3}. The IC_2021 is from 2021 samples collected at the National Kaohsiung University of Science and Technology (22°46'22.4" N 120°24'03.4" E) in Kaohsiung for the period of 8 – 18 December 2021. (diamond: mean value; outliers: < 1st quartile Q1-1.5 interquartile range (IQR) or > 3rd quartile Q3+1.5 IQR).

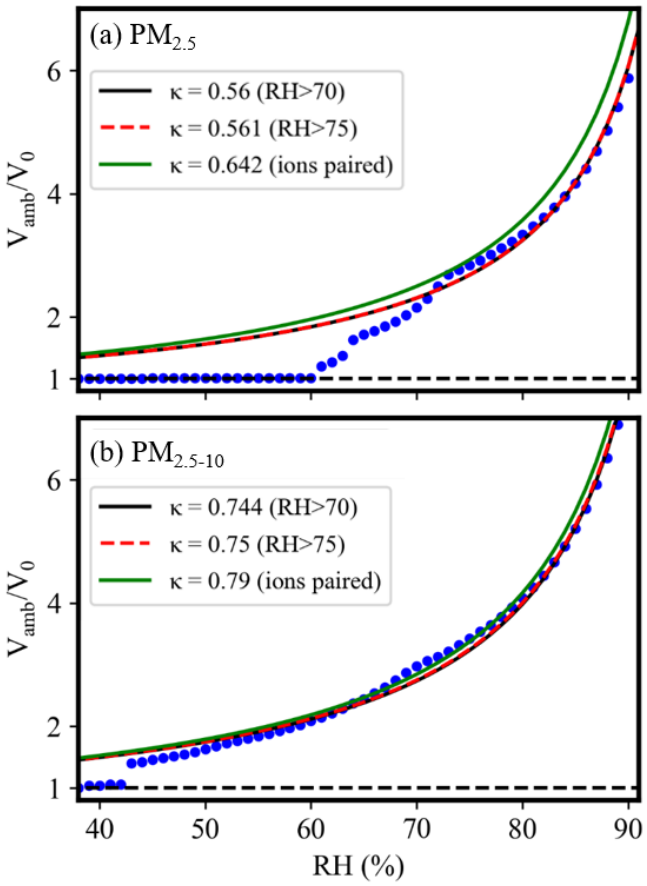

Figure S6: The volume ratio (ambient state compared to dry state) as a function of RH for (a) $PM_{2.5}$ and (b) $PM_{2.5-10}$ using E-AIM, along with the fitting lines using κ-Köhler equation (Eq. 2) with data points above the threshold as indicated in the legend. Sample mean composition with the molarity ratio of Na^+:NH_4^+:Cl^- :SO_4^{2-}:NO_3^- is 7:229:0:71:94 and 65:59:16:19:70 for $PM_{2.5}$ and $PM_{2.5-10}$, respectively. No insoluble composition is taken into account in the calculation.

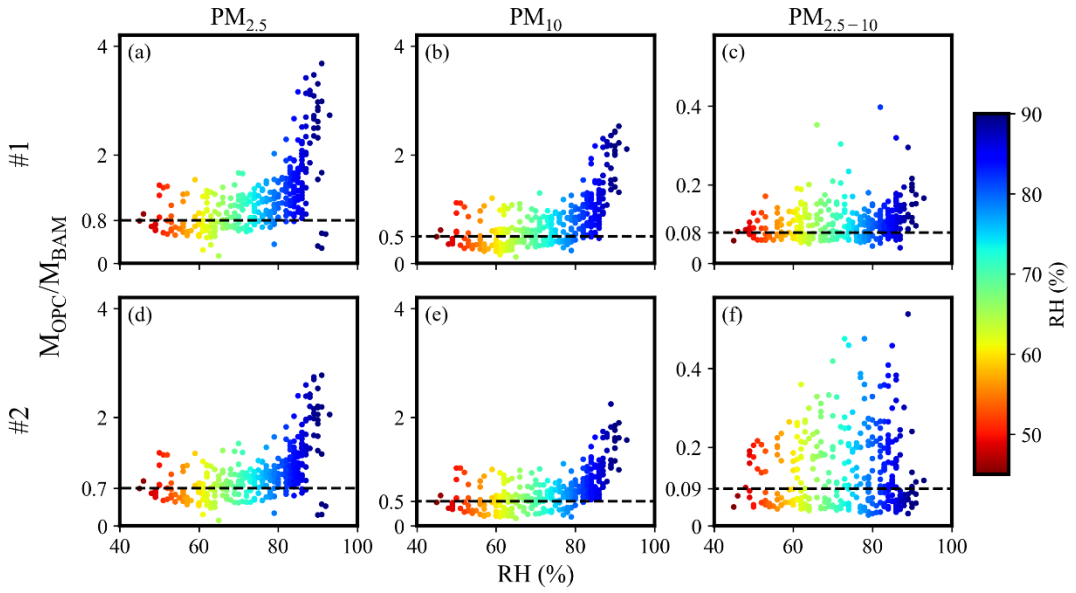

Figure S7: The mass ratio (ambient state compared to dry state) as a function of RH for (a, d) $PM_{2.5}$, (b, e) PM_{10}, and (c, f) $PM_{2.5-10}$ for AQB #1 and #2 data comparison. The marker color corresponds to RH. The dashed lines indicate the inverse of the sensitivity coefficient (α) obtained from data at RH ≤50%.

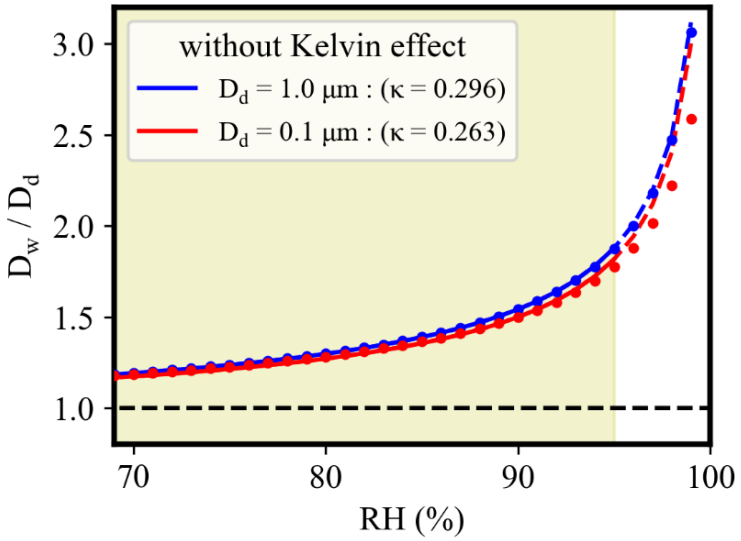

Figure S8: The particle growth diameter ratio as a function of RH for particle sizes of 0.1 μm (red) and 1.0 μm (blue). Points are diameter ratio with the Kelvin effect considered at κ = 0.3 for 70-95% of RH using Eq. 2, and solid lines are the fitting results for the points to derive κ without the Kelvin effect term.

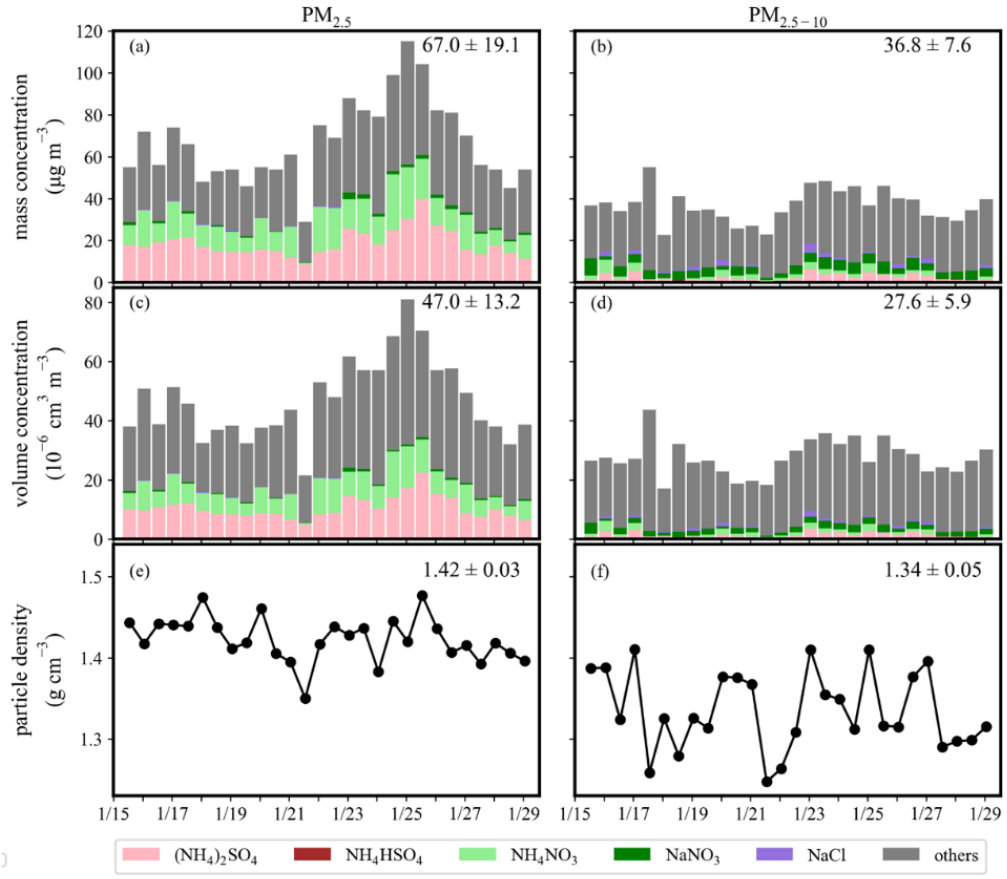

Figure S9: The temporal profiles of (a,b) mass and (c,d) volume concentration of chemical species from IC analysis and (e,f) calculated particle density for $PM_{2.5}$ and $PM_{2.5-10}$. The column color corresponds to the contribution of different components, with others characterized as secondary organic compositions having a density of 1.2 g cm^{-3}. The number on the upper right corner is the mean ± 1 SD.

References

Kim, A. H., Yum, S. S., Chang, D. Y., and Park, M.: Optimization of the sulfate aerosol hygroscopicity parameter in WRF-Chem, Geosci. Model Dev., 14, 259-273, 10.5194/gmd-14-259-2021, 2021.

Petters, M. D. and Kreidenweis, S. M.: A single parameter representation of hygroscopic growth and cloud condensation nucleus activity, Atmos. Chem. Phys., 7, 1961-1971, 10.5194/acp-7-1961-2007, 2007.

Xu, W., Ovadnevaite, J., Fossum, K. N., Lin, C., Huang, R. J., O'Dowd, C., and Ceburnis, D.: Aerosol hygroscopicity and its link to chemical composition in the coastal atmosphere of Mace Head: marine and continental air masses, Atmos. Chem. Phys., 20, 3777-3791, 10.5194/acp-20-3777-2020, 2020.